

# Consideration of Phase Transformations in the Study of Shear Bands in a Dynamically Loaded Steel Block

Z. G. Zhu

R. C. Batra  
Fellow ASME

Department of Mechanical and  
Aerospace Engineering  
and Engineering Mechanics,  
University of Missouri-Rolla,  
Rolla, MO 65401-0249

*We study plane strain thermomechanical deformations of a square block made of steel, and model a material defect in it by a rigid non-heat-conducting ellipsoidal inclusion located at the center of the block. The boundaries of the block are presumed to be thermally insulated, and its top and bottom surfaces compressed vertically at a prescribed rate. The loading pulse is assumed to be made up of three parts; an initial segment in which the speed increases from zero to the steady value, the steady part, and the third part in which the speed decreases gradually to zero and is maintained at zero subsequently. In the undeformed state, the specimen is assumed to be fully annealed, isotropic, and its microstructure to be a mixture of coarse ferrite and cementite. A material point is presumed to start transforming into austenite once its temperature exceeds the transformation temperature; the rate of transformation is controlled by a simple kinetic equation. Proper account is taken of the latent heat required for the transformation, the associated volume change, and the variation in the thermophysical properties. The complete thermomechanical problem is analyzed during the loading and unloading phase till all of the body points have essentially come to rest, and the energy equation is solved subsequently. It is found that the austenite is quenched rapidly enough by the surrounding material for it to be converted into martensite rather than pearlite or a mixture of pearlite and martensite.*

## Introduction

Shear bands in a dynamically loaded metal block often occur when softening caused by the heating of the material exceeds the combined effects of strain and strain-rate hardening, and generally precede shear fractures. These bands have been observed by Tresca (1878) and Massey (1921), who called them hot lines. Zener and Hollomon (1944) measured 32  $\mu\text{m}$  wide shear bands during the punching of a hole in a steel plate, and stated that some of the region within the band etched white, thereby suggesting the presence of martensite within the band. Roger (1979), in his review article, has alluded to similar observations and hypothesized that hot material within the band is quenched fast enough by the surrounding colder material that austenite within the band is transformed into martensite. Lindholm and Johnson (1983) have reported on the presence of martensite within a shear band formed in AMS6418 steel. Giovanola (1988) has measured temperatures close to 1100°C in shear bands formed in 4340 VAR (vacuum arc remelted) steel, which is well above the transformation temperature of ferrite and cementite into austenite. Wingrove (1971), based on electron microscopic observations, concluded that, indeed, transformation into martensite occurred within the band.

We note that previous analytical and numerical works (e.g., see Zhu and Batra (1990) for a list of references) on the analysis of shear bands in a dynamically loaded steel block did not consider the possibility of phase transformations. Here we postulate rather simple kinetic equations for the transformation of the mixture of ferrite and cementite into austenite during heating, and from austenite to martensite or pearlite during cooling. It is shown that the material within the band is indeed cooled fast enough by the surrounding material that the austenite is transformed into martensite, and the total time taken from the beginning of the loading phase to the cooling of the body to a nearly uniform temperature equals 150 milliseconds.

## Formulation of the Problem

We use a fixed set of rectangular Cartesian coordinates with origin at the centroid of the square block (cf. Fig. 1) to analyze its plane strain thermomechanical deformations. We assume that the block is made of steel, and in the stress-free reference configuration the material is fully annealed, isotropic, and its microstructure is a mixture of coarse ferrite and cementite. Furthermore, there is a non-heat-conducting rigid ellipsoidal inclusion with its major and minor axes coinciding with the centroidal axes of the cross-section. In terms of the referential description, governing equations are:

Contributed by the Materials Division for publication in the JOURNAL OF ENGINEERING MATERIALS AND TECHNOLOGY. Manuscript received by the Materials Division February 24, 1992; revised manuscript received March 22, 1992. Associate Technical Editor: D. Hui.

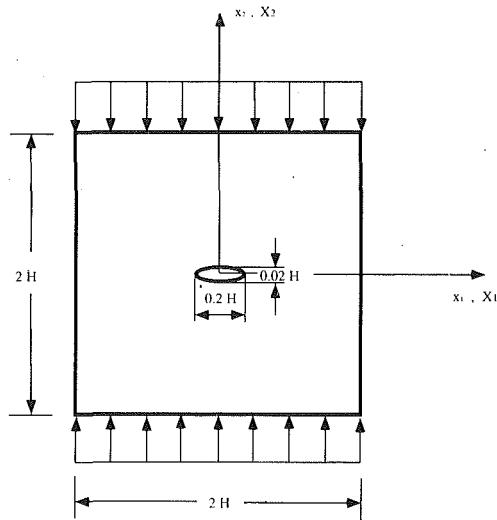


Fig. 1 A schematic sketch of the problem studied

$$(\rho J)^{\cdot} = 0, \quad (1)$$

$$\rho_0 \dot{v}_i = T_{i\alpha, \alpha}, \quad (2)$$

$$\rho_0 \dot{e} = -Q_{\alpha, \alpha} + T_{i\alpha} v_{i, \alpha} + \dot{Q}_L, \quad (3)$$

where

$$J = \det F_{i\alpha}, \quad F_{i\alpha} = x_{i, \alpha}, \quad x_{i, \alpha} = \partial x_i / \partial X_{\alpha}, \quad (4)$$

$x_i$  is the present location of a material particle that occupied place  $X_{\alpha}$  in the reference configuration,  $\rho$  its present mass density,  $\rho_0$  its mass density in the reference configuration,  $v_i$  its present velocity,  $T_{i\alpha}$  the first Piola-Kirchoff stress tensor,  $Q_{\alpha}$  the heat flux per unit reference area,  $e$  the specific energy, a superimposed dot indicates the material time derivative, and a repeated index implies summation over the range of the index. Equations (1), (2), and (3) express, respectively, the balance of mass, balance of linear momentum, and the balance of internal energy. For the constitutive relations we take

$$\sigma_{ij} = -B \left( \frac{\rho}{\rho_0} - 1 \right) \delta_{ij} + 2\mu D_{ij} - 3K(e_{th} + e_{ph}) \delta_{ij}, \quad (5.1)$$

$$T_{i\alpha} = \frac{\rho_0}{\rho} X_{\alpha, j} \sigma_{ij}, \quad 2\mu = \frac{\sigma_0}{\sqrt{3I}} (1 + bI)^m (1 - \nu(\theta - \theta_0)), \quad (5.2, 3)$$

$$2D_{ij} = v_{i, j} + v_{j, i}, \quad 2I^2 = \hat{D}_{ij} \hat{D}_{ij}, \quad \hat{D}_{ij} = D_{ij} - \frac{1}{3} D_{kk} \delta_{ij}, \quad (5.4, 5, 6)$$

$$Q_{\alpha} = \frac{\rho_0}{\rho} X_{\alpha, j} q_j, \quad q_i = -k\theta_{, i}, \quad (5.7, 8)$$

$$\rho_0 \dot{e} = \rho_0 c \dot{\theta} + \frac{\rho_0 \dot{\rho}}{\rho^2} \left[ B \left( \frac{\rho}{\rho_0} - 1 \right) + 3K(e_{th} + e_{ph}) \right], \quad (5.9)$$

$$e_{th} = 3 \int_{\theta_0}^{\theta} \hat{\alpha}(\theta) d\theta, \quad e_{ph} = \frac{\Delta v_{ph}}{\nu}, \quad (5.10, 11)$$

$$\frac{\Delta v_{ph}}{\nu} = - (f_{\gamma} + f_m) \xi_1 + f_m \xi_2,$$

$$\dot{Q}_L = \dot{Q}_{1L} + \dot{Q}_{2L} + \dot{Q}_{3L}. \quad (5.12, 13)$$

Here  $\sigma_{ij}$  is the Cauchy stress tensor,  $B$  may be thought of as the bulk modulus for the material of the block,  $K$  equals the bulk modulus,  $\mathbf{D}$  is the strain-rate tensor,  $\sigma_0$  the yield stress of the material in a quasistatic simple tension or compression test, parameters  $b$  and  $m$  characterize the strain-rate sensitivity of the material,  $I$  is the second invariant of the deviatoric strain-rate tensor  $\hat{\mathbf{D}}$ ,  $\nu$  is the coefficient of thermal softening,  $k$  equals

the thermal conductivity,  $c$  the specific heat,  $\theta$  the temperature rise of a material particle,  $\hat{\alpha}$  the coefficient of thermal expansion,  $\xi_1$  the dilatational strain for complete transformation of austenite ( $\gamma$ -phase) to pearlite or the strain of volume shrinkage for complete transformation of ferrite and cementite to austenite,  $\xi_2$  the dilatational strain for complete transformation of austenite to martensite,  $\dot{Q}_{1L}$  the rate of latent heat for the transformation from the mixture of ferrite and cementite to  $\gamma$ -phase,  $\dot{Q}_{2L}$  the rate of latent heat for the transformation from  $\gamma$ -phase to pearlite,  $\dot{Q}_{3L}$  is the rate of latent heat for the transformation of  $\gamma$ -phase to martensite,  $f_{\gamma}$  is the volume fraction of the  $\gamma$ -phase, and  $f_m$  the volume fraction of the martensite phase present at a spatial location. Batra (1988) and Batra and Liu (1989) have used Eq. (5.1) with  $\mu$  given by (5.3) to study the steady-state penetration problem and the initiation and growth of shear bands in a viscoplastic material. Batra and Jayachandran (1992) have shown that for the penetration problem, it and the constitutive relations proposed by Bodner-Partom (1975) and Brown et al. (1989) give essentially identical results. The last term on the right-hand side of Eq. (5.1) accounts for the pressure induced by dilatation associated with the phase changes, and should not affect plastic deformations of the body.

The thermophysical properties of a material point are determined from their values for different phases, the volume fractions of these phases making up that material particle, and the rule of mixtures. That is

$$\eta = f_{\alpha} \eta_{\alpha} + f_{\gamma} \eta_{\gamma} + f_m \eta_m \quad (6)$$

where  $\eta_{\alpha}$ ,  $\eta_{\gamma}$ , and  $\eta_m$  are the values of  $\eta$  for the  $\alpha$ -phase,  $\gamma$ -phase, and martensite, respectively. Strictly speaking, the  $\alpha$ -phase is ferrite. For simplicity, we take the material properties of the mixture of ferrite and cementite to be the same as that of pearlite, also referred to as the  $\alpha$ -phase. We note that the three phases need not be present simultaneously at a point. Budiansky (1970) has derived expressions for thermophysical parameters for an isotropic composite in terms of volume fractions and thermophysical constants of the constituents. Inoue (1989) has obtained expressions for Young's modulus, Poisson's ratio, the coefficient of thermal expansion, and the volumetric dilatation due to phase changes for the mixture in terms of the values of these parameters for the constituents and their volume fractions. Of these, the global values of the coefficient of thermal expansion and the volumetric dilatation obey Eq. (6). Inoue (1989) has assumed an expression like Eq. (6) for the potential (or yield) function for a mixture. Here, for simplicity, we use Eq. (6) to evaluate all of the material parameters needed in this study.

The kinetic equation for the phase transformation from the  $\alpha$ -phase to the  $\gamma$ -phase is taken to be

$$\dot{f}_{\gamma} = \begin{cases} \frac{\dot{\theta}}{25}, & \text{for } \dot{\theta} > 0, 725^{\circ}\text{C} \leq \theta \leq 750^{\circ}\text{C}, \\ 0, & \text{otherwise.} \end{cases} \quad (7.1)$$

Thus

$$f_{\gamma} = (\theta - 725)/25, \quad \text{for } \dot{\theta} > 0, 725^{\circ}\text{C} \leq \theta \leq 750^{\circ}\text{C}. \quad (7.2)$$

Similarly, the latent heat release rate for the transformation from  $\alpha$ -phase to  $\gamma$ -phase is assumed to have the form

$$\dot{Q}_{1L} = \begin{cases} -\frac{\dot{\theta}}{25} Q_1, & 725^{\circ}\text{C} \leq \theta \leq 750^{\circ}\text{C}, \dot{\theta} > 0, \\ 0, & \text{otherwise.} \end{cases} \quad (8)$$

Whether or not  $\gamma$ -phase changes back to  $\alpha$ -phase depends upon the cooling rate at a point. Referring to Fig. 2, the transformation from  $\gamma$ -phase to pearlite is assumed to begin as soon as the cooling curve for a point intersects parabola  $A$ , and is presumed to have completed by the time the cooling

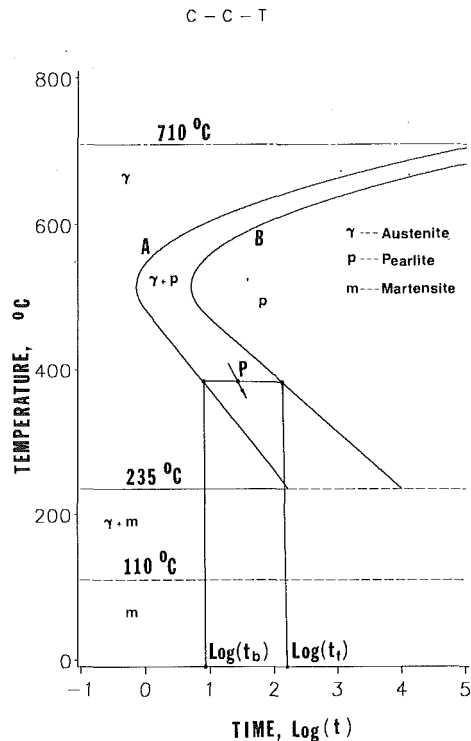


Fig. 2 Phase diagram during continuous cooling for a typical steel

curve intersects parabola  $B$ . At any intermediate point  $P$ , we assume that the rate of conversion from  $\gamma$ -phase to pearlite and the corresponding rate of release of the latent heat are given by

$$\dot{f}_\alpha = \frac{\hat{k}}{\ln 10} \max\left(\frac{1}{\log t'}, \frac{1}{t_{\text{eff}}}\right), \quad t' = t - t^* > t_b, \quad (9)$$

$$\dot{Q}_{3L} = Q_{3L} \dot{f}_\alpha, \quad (10)$$

where

$$\hat{k} = \frac{1}{t_f - t_b}, \quad (11.1)$$

$$t_{\text{eff}} = t_b^{1 - f_\alpha} t_f^{f_\alpha}, \quad (11.2)$$

$t_b$  and  $t_f$  are defined in Fig. 2, and  $t^*$  equals the time when the temperature reaches  $710^\circ\text{C}$  during the cooling process. Thus, we assume that  $f_\alpha$  increases linearly from 0 to 1 between times  $\log t_b$  and  $\log t_f$ . Note that the abscissa in Fig. 2 equals the logarithm of time.

If the temperature of a material point where  $\gamma$ -phase is present reaches  $235^\circ\text{C}$  during the cooling process, we assume that the  $\gamma$ -phase starts transforming into martensite, the rate of transformation and the rate of latent heat release being given by

$$\dot{f}_m = \begin{cases} -\frac{1}{125} f_\gamma^* \dot{\theta}, & \dot{\theta} < 0, \quad 110^\circ\text{C} \leq \theta \leq 235^\circ\text{C}, \\ 0, & \text{otherwise,} \end{cases} \quad (12)$$

$$\dot{Q}_{3L} = Q_{3L} \dot{f}_m. \quad (13)$$

Here  $f_\gamma^*$  equals the volume fraction of the  $\gamma$ -phase present at the material particle when its temperature cools down to  $235^\circ\text{C}$ .

Inoue (1989), in his review article, has summarized a theory of elastoviscoplasticity that incorporates the effect of phase transformations, and has also listed kinetic equations for phase transformations used by different investigators. These kinetic equations are considerably more involved than Eqs. (7.1), (9), and (12), and require a knowledge of material parameters not

available in any handbook. The constitutive relations (7.1), (9), and (12) are based on the observations from the phase diagram, which indicate that ferrite transforms into austenite at about  $725^\circ\text{C}$ , and that above this temperature, and depending upon the carbon content, different volume fractions of these phases may be in equilibrium. Thus, one will need to know the initial carbon content and also study the diffusion of carbon. Such details are warranted in the analysis of the mechanics of phase transformations; however, we omit these herein. Realizing that the phase diagram refers to the equilibrium situation and the transformation from one phase to another does not occur instantaneously, we have taken (7.1), (9), and (12) as the constitutive relations for  $\dot{f}_\gamma$  and  $\dot{f}_\alpha$ .

We introduce non-dimensional variables, indicated below by a superimposed bar, as follows.

$$\bar{\sigma} = \sigma/\sigma_r, \quad \bar{s} = s/\sigma_r, \quad \bar{T} = T/\sigma_r, \quad \bar{B} = B/\sigma_r, \quad \bar{K} = K/\sigma_r,$$

$$\bar{Q}_L = Q_L/\sigma_r, \quad \bar{x} = x/H, \quad \bar{X} = X/H, \quad \dot{\gamma}_0 \equiv v_0/H, \quad \bar{v} = v/v_0,$$

$$\bar{I} = I/\dot{\gamma}_0, \quad \bar{D} = D/\dot{\gamma}_0, \quad \bar{t} = t\dot{\gamma}_0, \quad \bar{b} = b\dot{\gamma}_0, \quad \bar{\nu} = \nu\theta_r, \quad \theta_r \equiv \frac{\sigma_r}{\rho_r c_r},$$

$$\bar{\alpha} = \alpha\theta_r, \quad \bar{\rho} = \rho/\rho_r, \quad \bar{\rho}_0 = \rho_0/\rho_r, \quad \bar{c} = c/c_r, \quad \delta \equiv \rho_r v_0^2/\sigma_r,$$

$$\beta = \frac{k_r}{\rho_r c_r v_0 H}, \quad \bar{k} = k/k_r. \quad (14)$$

The subscript  $r$  on a quantity indicates its reference value, usually that for the initial ferrite and cementite phases,  $2H$  equals the length of a side of the square cross-section,  $v_0$  is the value of the steady velocity applied on the top and bottom surfaces, and  $\dot{\gamma}_0$  equals the average applied strain rate. Henceforth, we work in terms of nondimensional variables and drop the superimposed bar. We note that the nondimensional number  $\delta$  indicates the importance of inertia forces relative to the yield stress of the material, and  $\beta$  equals the thermal length.

We assume that all four sides of the square cross-section are thermally insulated, the two vertical sides are traction free, there is no tangential traction on the top and bottom edges, and a preassigned vertical velocity is prescribed on these edges. Thus, it is reasonable to assume that the deformations of the block are symmetrical about the horizontal and vertical centroidal axes. We study deformations of the material lying in the first quadrant and impose on it the following boundary conditions.

$$v_1 = 0, \quad T_{12} = 0, \quad Q_1 = 0 \quad \text{at} \quad x_1 = X_1 = 0, \quad (15.1)$$

$$v_2 = 0, \quad T_{21} = 0, \quad Q_2 = 0 \quad \text{at} \quad x_2 = X_2 = 0, \quad (15.2)$$

$$T_{11} = 0, \quad T_{12} = 0, \quad Q_1 = 0 \quad \text{on} \quad X_1 = H, \quad (15.3)$$

$$T_{12} = 0, \quad v_2 = -h(t), \quad Q_2 = 0 \quad \text{on} \quad X_2 = H, \quad (15.4)$$

$$v_1 = 0, \quad v_2 = 0, \quad Q_\alpha N_\alpha = 0$$

$$\text{on the surface of the rigid inclusion.} \quad (15.5)$$

The boundary conditions on the edges  $X_1 = 0$  and  $X_2 = 0$  follow from the presumed symmetry of deformations, and those on the inclusion surface are implied by the assumptions that the inclusion is rigid and non-heat-conducting. The function  $h(t)$  is given by

$$h(t) = t/0.005, \quad 0 \leq t \leq 0.005, \quad (16.1)$$

$$= 1, \quad 0.005 \leq t \leq 0.5055, \quad (16.2)$$

$$= 1 - \frac{t - 0.5055}{0.005}, \quad 0.5055 \leq t \leq 0.5105, \quad (16.3)$$

$$= 0, \quad t \geq 0.5105. \quad (16.4)$$

The duration of the loading pulse is believed to be large enough to cause the phase transformation from  $\alpha$ -phase to  $\gamma$ -phase to occur. It will be interesting to see if the cooling of austenite due to the heat loss from the material within the band to the

surrounding material is rapid enough to facilitate its transformation into martensite or not.

For the initial conditions, we take

$$\rho(\mathbf{x},0) = 1, \quad \mathbf{v}(\mathbf{x},0) = \mathbf{0}, \quad \theta(\mathbf{x},0) = \theta_0, \quad f_\alpha(\mathbf{x},0) = 1.0, \\ f_\gamma(\mathbf{x},0) = 0, \quad f_m(\mathbf{x},0) = 0. \quad (17)$$

That is, the body is initially at rest, has a uniform mass density and temperature, and all of the material is a mixture of ferrite and cementite.

### Computational Considerations

The problem formulated above is highly nonlinear. It is almost impossible to prove the existence and uniqueness of its solution. Here we find an approximate solution of the problem by first reducing the coupled nonlinear partial differential equations governing the thermomechanical deformations of the block to a set of coupled, nonlinear, and ordinary stiff differential equations by using the Galerkin approximation. At each node point in the mesh, two components of the velocity, the temperature and the mass density are taken as unknowns. A finite element mesh consisting of 4-noded quadrilateral elements with  $2 \times 2$  Gauss quadrature rule and lumped mass matrix is employed. The stiff ordinary differential equations are integrated with respect to time by using the backward difference Adam's method included in the subroutine LSODE (e.g., see Hindmarsh, 1971). The Gear method, also included in LSODE, could not be used because of the limited core storage available. The computer code developed by Batra and Liu (1989) was suitably modified to solve the present problem.

The temperature at a quadrature (Gauss) point within an element is computed from a knowledge of its values at the node points. The temperature and its rate of change at a quadrature point determine, according to Eqs. (7.1), (9), and (12), the phase transformation at that point. The value of a thermophysical property at a quadrature point is determined by using Eq. (6).

### Results and Discussion

We assume that in the unstressed reference configuration the microstructure is a mixture of coarse ferrite and cementite, and assign the following values to various parameters. Parameters that are taken to have the same value for all three phases are indicated without any subscripts.

$$b = 10,000 \text{ s}, \quad \rho_r = 7860 \text{ kg m}^{-3}, \quad B = 128 \text{ GPa}, \\ c = 473 \text{ J kg}^{-1} \text{ }^\circ\text{C}^{-1}, \quad v_0 = 25 \text{ m/s}, \quad H = 5 \text{ mm}, \\ \theta_0 = 25 \text{ }^\circ\text{C}, \quad K = 159(1 - 1.47 \times 10^{-4} \theta) \text{ GPa}, \\ -Q_{1L} = Q_{2L} = 0.628 \times 10^9 \text{ Jm}^{-3}, \quad Q_{3L} = 0.542 \times 10^9 \text{ Jm}^{-3}, \\ e_{ph}^{\alpha\alpha} = -e_{ph}^{\alpha\gamma} = 0.007, \quad e_{ph}^{\gamma m} = 0.044, \quad \xi_1 = 0.007, \quad \xi_2 = 0.044, \\ \alpha_\alpha = 14 \times 10^{-6} \text{ }^\circ\text{C}^{-1}, \quad \alpha_\gamma = 21 \times 10^{-6} \text{ }^\circ\text{C}^{-1}, \\ \alpha_m = 13 \times 10^{-6} \text{ }^\circ\text{C}^{-1}, \\ k_\alpha = 49.216(1 - 5.05 \times 10^{-4} \theta) \text{ Wm}^{-1} \text{ }^\circ\text{C}^{-1}, \\ k_\gamma = 15(1 + 7.48 \times 10^{-4} \theta) \text{ Wm}^{-1} \text{ }^\circ\text{C}^{-1}, \\ k_m = 43.1(1 - 5.03 \times 10^{-4} \theta) \text{ Wm}^{-1} \text{ }^\circ\text{C}^{-1}, \\ \sigma_r = \sigma_{0\alpha} = 333 \text{ MPa}, \quad \sigma_{0\gamma} = 190 \text{ MPa}, \quad \sigma_{0m} = 1600 \text{ MPa}, \\ \nu_m = 2.5 \times 10^{-4} \text{ }^\circ\text{C}^{-1}, \\ \text{for } 0 \leq \theta \leq 600 \text{ }^\circ\text{C}, \quad \nu_\alpha = 1.51 \times 10^{-3} \text{ }^\circ\text{C}^{-1}, \\ \nu_\gamma = 1.392 \times 10^{-3} \text{ }^\circ\text{C}^{-1}, \\ \text{for } \theta > 600 \text{ }^\circ\text{C}, \quad \nu_\alpha = 1.11 \times 10^{-4} \text{ }^\circ\text{C}^{-1}, \\ \nu_\gamma = 1.83 \times 10^{-4} \text{ }^\circ\text{C}^{-1}. \quad (18)$$

Here we have made an exception to our notation and indicated

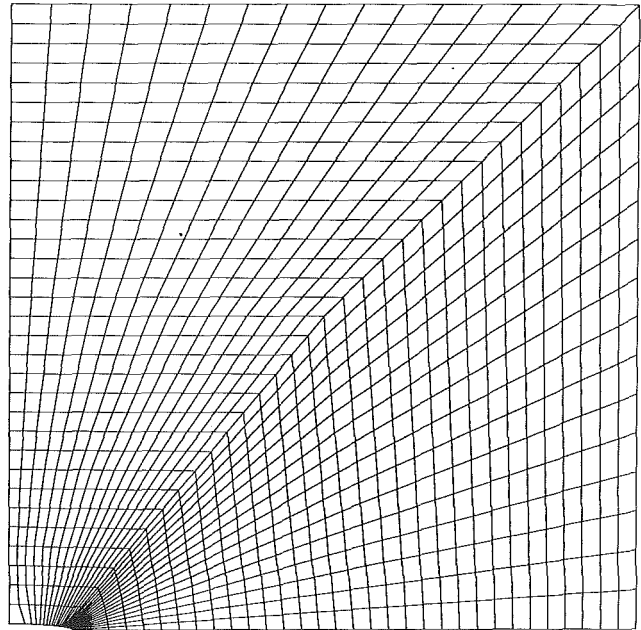


Fig. 3 Discretization of the domain into the finite element mesh used to analyze the problem

dimensional quantities to clarify units used. The value of the temperature  $\theta$  in expressions for several variables is measured in  $^\circ\text{C}$ . For assigned values of  $v_0$  and  $H$ , the average applied strain-rate equals  $5000 \text{ sec}^{-1}$ . The superscripts  $\gamma\alpha$  and  $\gamma m$  on  $e_{ph}$  indicate that the volumetric strain for complete transformation from  $\gamma$ -phase to pearlite and from  $\gamma$ -phase to martensite equal 0.007 and 0.044, respectively. Values of material parameters associated with different phases are taken from Reed-Hill (1973) and Yu et al. (1979).

Figure 3 depicts the discretization of the domain into the finite element mesh used to analyze the problem. The mesh is fine in regions adjoining the tip of the ellipsoidal inclusion where severe deformations are expected to occur. Since we use an updated Lagrangian description of motion, the spatial coordinates of nodes are updated after every time increment. The size of the time increment is selected adaptively by the subroutine LSODE in order to solve the given problem within the prescribed accuracy during each time increment. Herein the values of the absolute and relative tolerances required by LSODE were each set equal to  $10^{-2}$ . Since the analytical solution of the problem is unknown, it is impossible to estimate the total error in the solution at any instant. During the course of the solution of the problem the deformed region had to be remeshed twice; this was indicated by the negative value of the Jacobian at a Gauss point. The values of the solution variables at nodes in the new mesh were obtained first by finding to which elements in the previous mesh these nodes belonged, and then using an interpolation technique.

Figure 4 depicts contours of the maximum principal logarithmic strain  $\epsilon$ , defined as,

$$\epsilon = \ln \lambda_1$$

where  $\lambda_1^2$  is the largest eigenvalue of the left or right Cauchy-Green tensor, at four different values of the nondimensional time  $t$ . These contours are plotted in the referential description and suggest that the material around the tip of the ellipsoidal inclusion deforms severely, and these intense deformations propagate along directions making an angle of nearly  $\pm 45$  deg with the horizontal. In order to decipher clearly the magnitude of deformations in different regions, we have plotted in Fig. 5 the evolution of the maximum principal logarithmic strain

at several points; the approximate locations of these points are given in Fig. 5(a). Point 1 adjoins the inclusion tip, points 36, 2, 38, and 3 are on the horizontal line through point 1 and situated in that order from point 1; points 31, 37, and 32 are vertically above points 36, 2, and 38, respectively. Since the ordinate is  $\ln \lambda_1$ , the maximum stretch at point 2 exceeds 12. The deformations at points 2, 31, and 37 eventually become larger than those at points 1 and 36, implying thereby that the severest deformations occur at points a little bit away from the inclusion tip. Intense deformations of the region surrounding point 17 seem to propagate vertically more than along the line passing through points 17 and 21. For comparison purposes we have also plotted the evolution of  $\epsilon$  at point 35, which is far removed from the inclusion tip. The value of the maximum principal logarithmic strain at point 35 evolves slowly in the beginning, and its rate of growth picks up at an average strain of 0.375. However, its overall deformations remain minuscule as compared to the deformations of the material surrounding point 2.

The evolution of the nondimensional temperature and the effective deviatoric stress  $s_e$  at several points is shown in Figs. 6 and 7, respectively. The effective stress  $s_e$  is given by

$$s_e = \left( \frac{1}{2} \text{tr}(ss^T) \right)^{1/2} = \frac{\sigma_0}{\sqrt{3}} (1 + bI)^m (1 - \nu(\theta - \theta_0)), \quad (19a)$$

where

$$\mathbf{s} = \sigma - \frac{1}{3} \sigma_{kk} \mathbf{1}. \quad (19b)$$

The sharp drop in the value of the effective stress at points 1, 2, 5, and 36 signifies the phase transformation from  $\alpha$ -phase to  $\gamma$ -phase there, since  $\sigma_0$  for the  $\gamma$ -phase is considerably lower than that for the mixture of ferrite and cementite. Thus, the material at point 36 is transformed into austenite first, followed by that at points 1, 2, and 5. Once the speed of material particles on the top surface has been reduced to zero, the average strain remains constant subsequently. However, the effective stress at these points does change, and will increase substantially once the phase transformation from austenite to martensite takes place. However, these changes are not shown in Fig. 7.

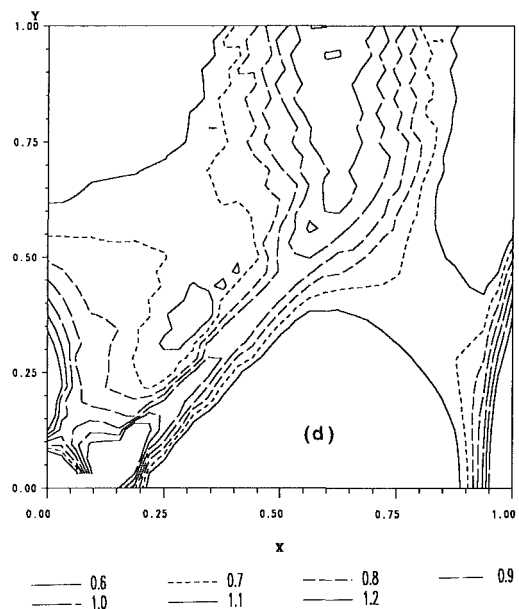
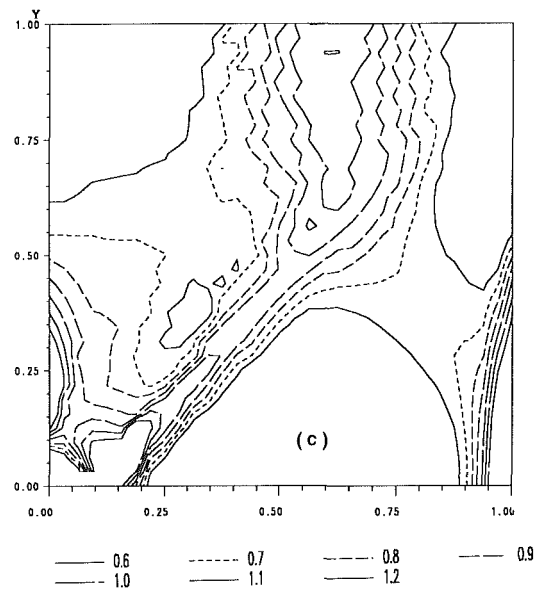
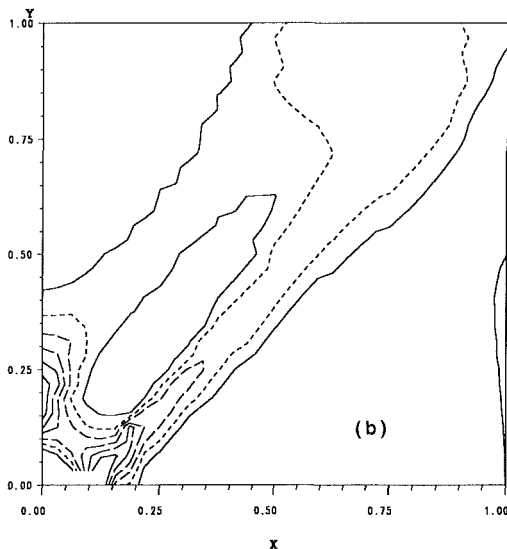
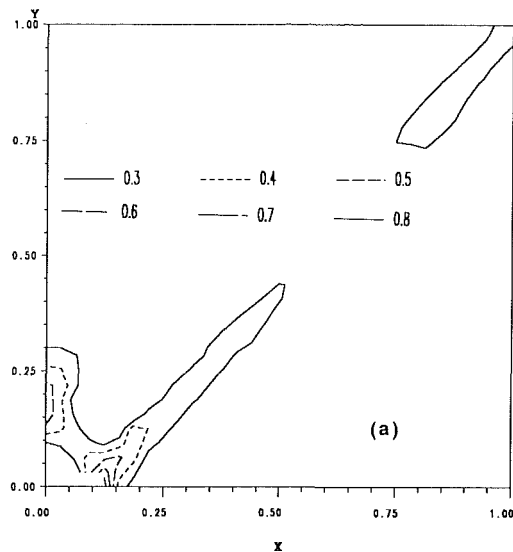


Fig. 4 Contours of the maximum principal logarithmic strain at four different values of the nondimensional time  $t$ . (a)  $t = 0.1687$ , (b)  $t = 0.2523$ , (c)  $t = 0.5105$ , and (d)  $t = 0.6710$ .

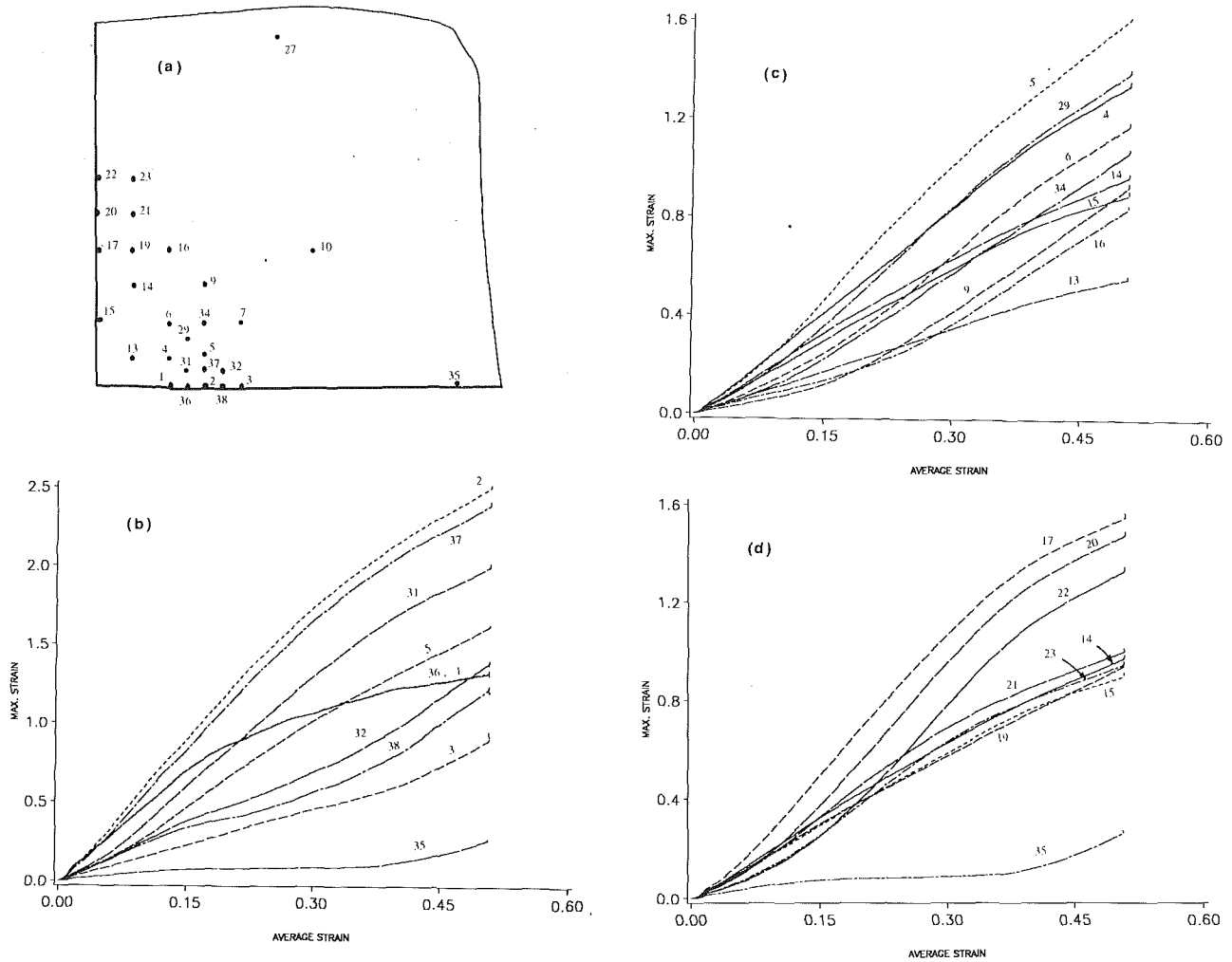


Fig. 5 Evolution of the maximum principal logarithmic strain at several points; the approximate location of these points is also shown

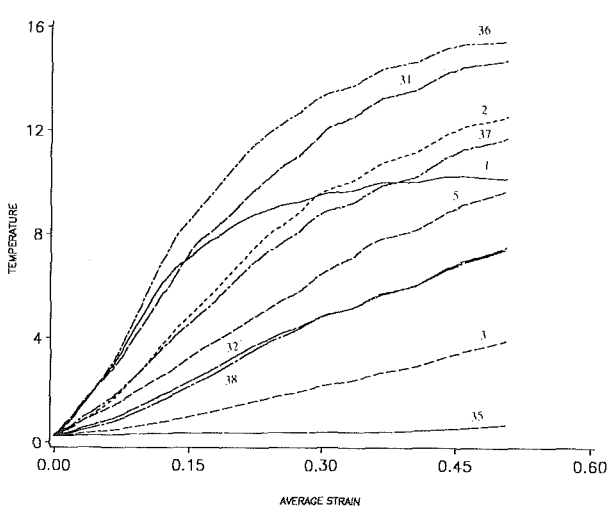


Fig. 6 Evolution of the nondimensional temperature at several points; the approximate location of these points is shown in Fig. 5

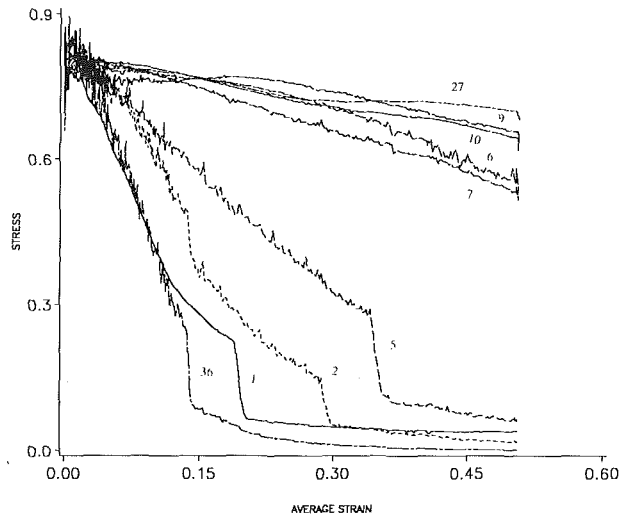


Fig. 7 Evolution of the effective stress at numerous points whose approximate locations are shown in Fig. 5

The values of the nondimensional temperature need to be multiplied by  $89.6^{\circ}\text{C}$  to obtain their corresponding values in  $^{\circ}\text{C}$ . Whereas the temperature at point 1 seems to level off, that at other points continues to increase. Zhu and Batra (1990) stud-

ied a similar problem earlier in which no account was taken of the phase transformations, all of the material parameters were assumed not to depend upon temperature and the softening of the material due to its being heated up was modeled

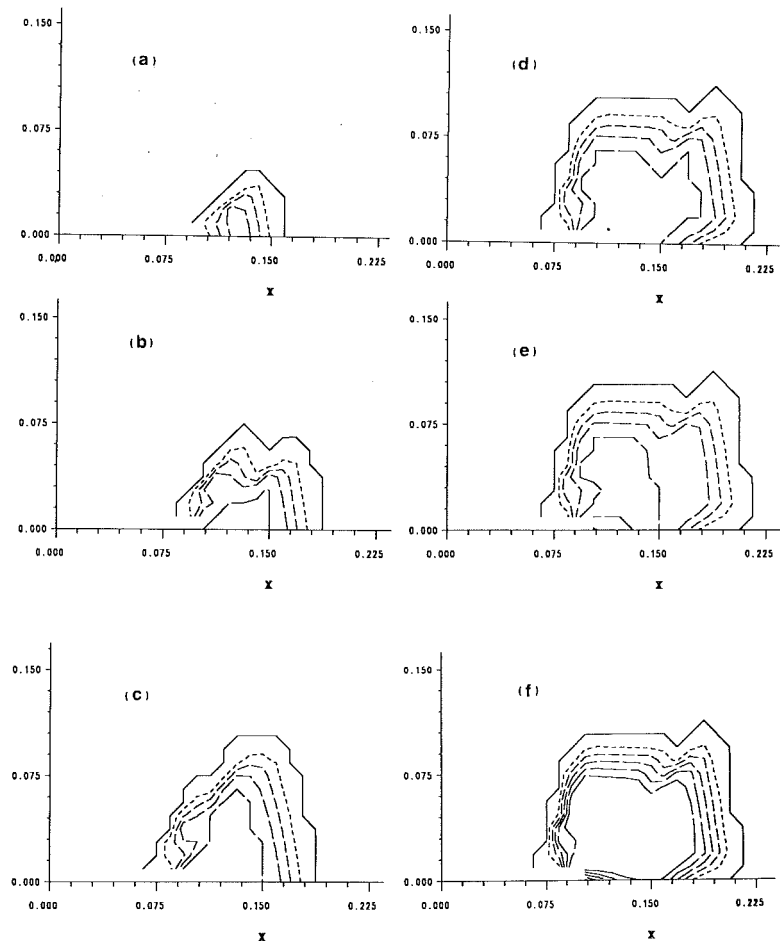


Fig. 8 Contours of the volume fraction of austenite at different values of time  $t$ . (a)  $t = 33.7 \mu\text{s}$ , (b)  $t = 67.5 \mu\text{s}$ , (c)  $t = 102 \mu\text{s}$ , (d)  $t = 134 \mu\text{s}$ , (e)  $t = 29.8$  milliseconds (ms), and (f)  $t = 99.9$  ms. —  $f_\gamma = 0.0$ , .....  $f_\gamma = 0.25$ , ---  $f_\gamma = 0.5$ , - · -  $f_\gamma = 0.75$ , — — —  $f_\gamma = 1.0$ .

by an exponential rather than a linear function. In that case (cf. Fig. 9(a) of Zhu and Batra, 1990), the temperature at point 1 was always higher than that at other points surrounding it, and the maximum principal logarithmic strain  $\epsilon$  at point 1 increased sharply once a shear band initiated. A glance at Fig. 5 shows that  $\epsilon$  at point 1 levels off, and there is no transition in the rate of growth of  $\epsilon$ . In the present problem it is hard to decipher when a shear band initiated.

In Fig. 8 we have plotted, in the reference configuration, contours of the volume fraction of austenite at time  $t$  equal to  $33.7 \mu\text{s}$ ,  $67.5 \mu\text{s}$ ,  $102 \mu\text{s}$ ,  $134 \mu\text{s}$ ,  $29.8$  millisecc (ms), and  $99.5$  ms. The horizontal and vertical scales have been enlarged to clarify the contours. We recall that the vertical velocity on the top surface is reduced to zero at  $t = 102 \mu\text{s}$ , and is kept at zero subsequently. Thus, no external work is done on the system for  $t \geq 102 \mu\text{s}$ , and the heat conduction from the hotter to the colder regions tends to equilibrate the temperature everywhere. All material particles had essentially come to rest at  $t = 134 \mu\text{s}$ , and only the heat equation was solved for  $t \geq 134 \mu\text{s}$ . Since we have assumed a simple kinetic equation for the phase transformation from  $\alpha$  to  $\gamma$  phase, some of the material is converted into austenite even after the top surface is brought to and maintained at rest. A comparison of the contours of the volume fraction of austenite with those of the maximum principal logarithmic strain reveals that some of the material outside of the shear band has also transformed into austenite. We do not get a very sharp and narrow band, primarily because the finite element mesh used is not very fine. The available

computational resources limited the size of the problem, and hence the mesh that could be used to analyze it.

Whether or not austenite is transformed into pearlite or into martensite depends upon how fast heat can be conducted out of the hotter regions by the surrounding colder material. Figure 9 depicts the variation of the temperature at point  $P$  with coordinates (0.1, 0.0368) in the reference configuration. The cooling curve for this point is also plotted on the C-C-T (continuous-cooling-transformation) diagram. The peak temperature at point  $P$  reached almost  $1075^\circ\text{C}$ , which is well above  $750^\circ$ , the temperature at which the transformation is assumed to have completed. Since the cooling curve for  $P$  does not intersect parabola A on the C-C-T diagram, the austenite present at point  $P$  is transformed directly into martensite. Similar reasoning applied at several points indicated that quenching of the hotter material caused by the surrounding colder material was strong enough to cause austenite to be transformed directly into martensite. The contours, in the reference configuration, of the volume fraction of martensite at four different values of time are exhibited in Fig. 10. The horizontal and vertical scales have been expanded to distinguish among the different contours. These plots evidence that a significant portion of austenite has been transformed into martensite. Because of the thermally insulated boundaries, the block cools down to a uniform temperature which is above  $110^\circ\text{C}$ . Therefore, all of the austenite cannot be transformed into martensite. However, if the block boundaries were able to exchange heat with the surroundings, then the material will cool down to the

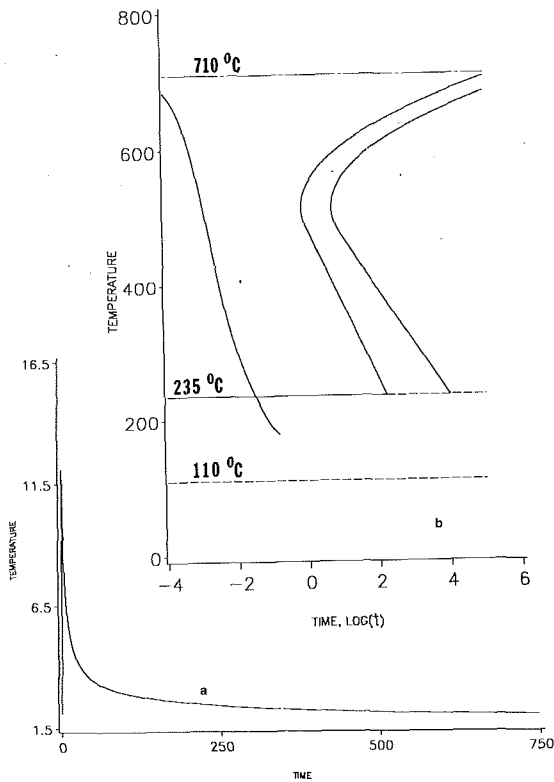


Fig. 9 (a) Variation of temperature with time at point P (0.1, 0.0368), (b) Cooling curve for point P superimposed on the C-C-T diagram.

room temperature eventually. The cooling curve for a typical point, shown in Fig. 9, indicates that it will not intersect either one of the two parabolas; the same was found to be the case for other points considered. Therefore, all of the austenite at a point will be transformed into martensite. Figure 10(e) shows contours of martensite for this case. The temperature contours at four different times, depicted in Fig. 11, reveal that only a small region near the inclusion tip is heated up significantly, and that the temperature distribution within the block becomes essentially uniform at time  $t = 99.9$  ms.

A similar study conducted at an average strain-rate of  $1000 \text{ s}^{-1}$  gave results qualitatively similar to the ones reported herein. The main reason for our not getting narrow shear bands is that the finite element mesh used is not fine enough. As stated earlier, a fine mesh could not be used because of the limited computing resources available. A fine mesh should result in sharper gradients of temperature across the shear band, and possibly higher values of temperature within it, thus facilitating the transformation from  $\alpha$ -phase to  $\gamma$ -phase. Here we have not accounted for the effect of the stress and/or strain on the phase transformations; Inoue (1989) has given kinetic equations for such phase transformations.

### Conclusions

We have analyzed plane strain thermomechanical deformations of a steel block of square cross-section and loaded in compression at an average strain-rate of  $5000 \text{ s}^{-1}$ . Hardening of the material due to strain-rate effects and its softening caused by its being heated up are accounted for. We have also considered the possible transformation of the material from the mixture of ferrite and cementite to  $\gamma$ -phase and back into

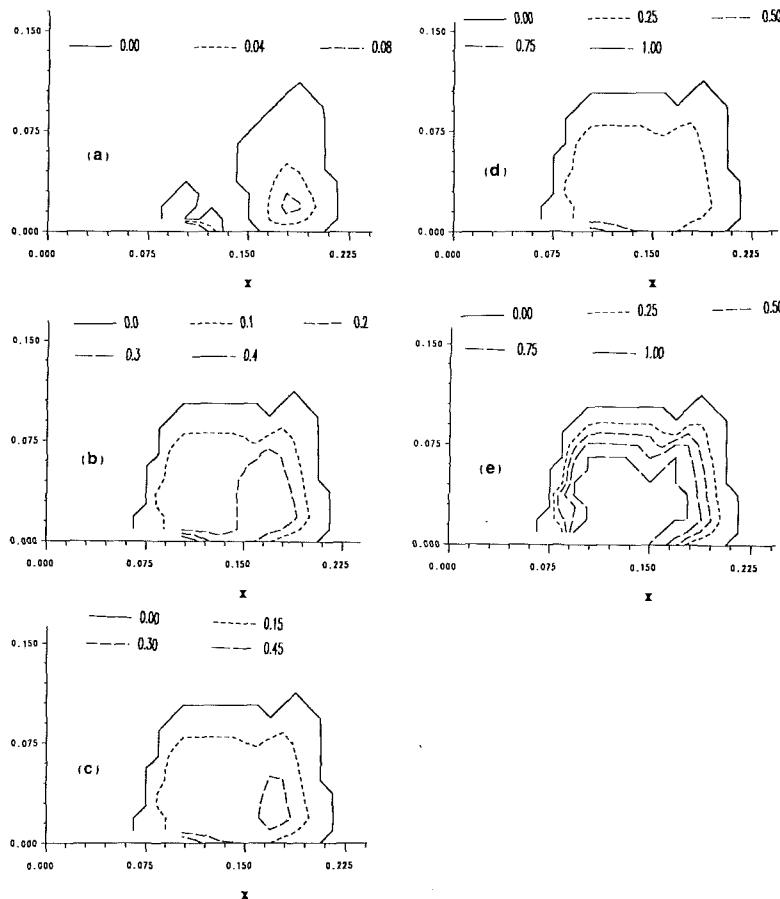


Fig. 10 Contours of the volume fraction of martensite at four different values of time  $t$ . (a)  $t = 29.8$  ms, (b)  $t = 49.8$  ms, (c)  $t = 59.8$  ms, (d)  $t = 99.9$  ms. (e) Contours of the volume fraction of martensite if all of the block had cooled down to the room temperature of  $25^\circ\text{C}$ .

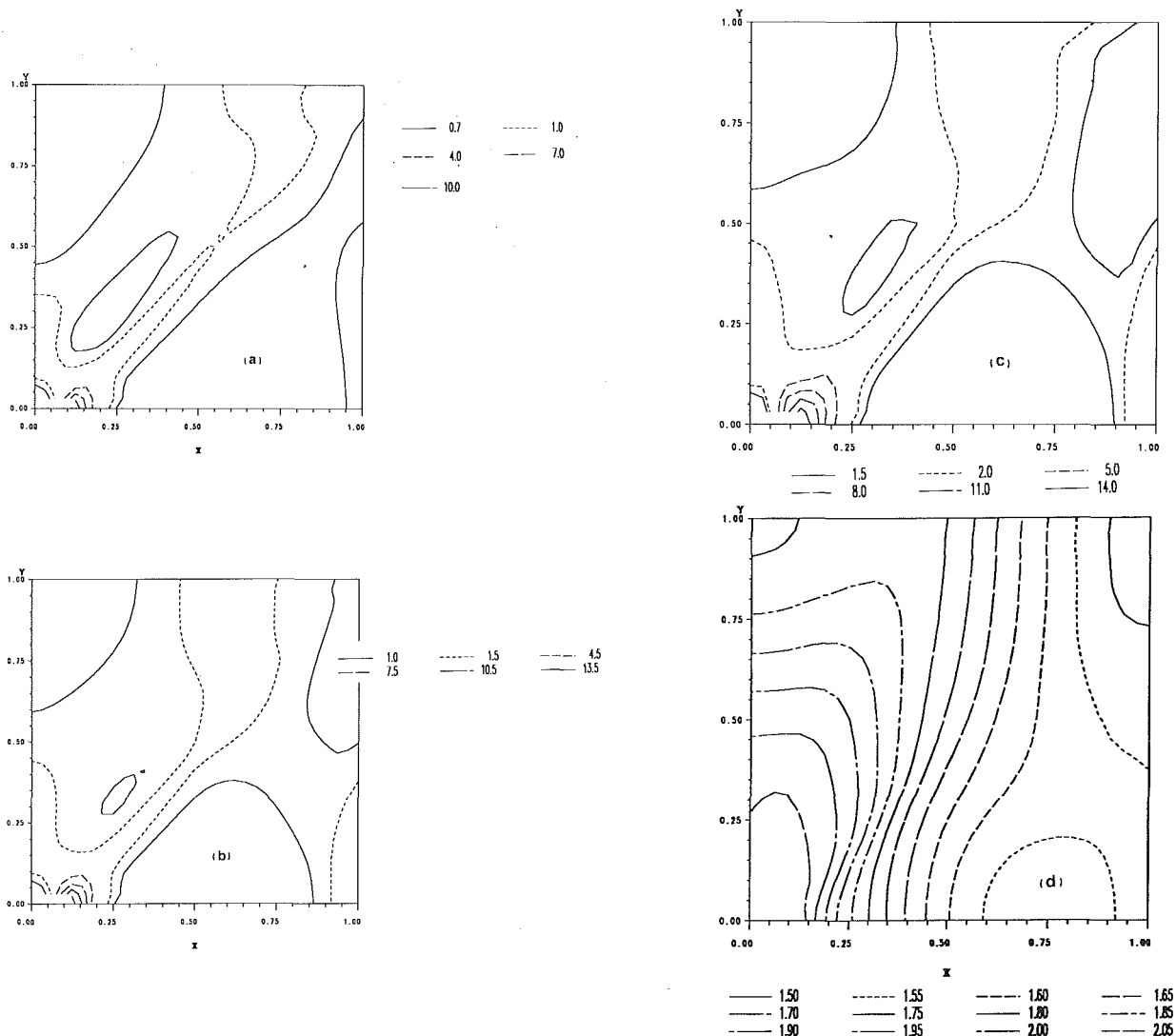


Fig. 11 Contours of temperature at four different values of time  $t$ . (a)  $t = 50.5 \mu\text{s}$ , (b)  $t = 84.5 \mu\text{s}$ , (c)  $t = 134 \mu\text{s}$ , and (d)  $t = 99.9 \text{ ms}$ .

either pearlite or martensite. The thermophysical properties of a material point consisting of more than one phase are determined by the rule of mixtures. The loading pulse is made up of an initial transient loading part of  $1 \mu\text{s}$  duration, a steady part of  $100 \mu\text{s}$ , and the unloading part of  $1 \mu\text{s}$ ; subsequently, the bottom and top surfaces are held fixed. A material defect is modeled by a rigid non-heat-conducting ellipsoidal inclusion located at the block center. The deformations are presumed to be symmetrical about the centroidal axes parallel to the bounding faces, and thus deformations of the material in the first quadrant are studied.

It is found that a narrow band of intense plastic deformation initiates at the inclusion tip and propagates along directions making an angle of approximately  $\pm 45 \text{ deg}$  with the horizontal. Much of the material within and adjoining the band is heated up to a temperature above  $725^\circ\text{C}$ , where the transformation from the mixture of ferrite and cementite to the  $\gamma$ -phase is presumed to begin. This hotter material is quenched by the cold material surrounding it at a rapid enough rate that the  $\gamma$ -phase is transformed directly into martensite.

#### Acknowledgments

This work was supported by the U.S. Army Research Office

grant DAAL03-91-G-0084 and the U.S. NSF grant MSS9121279 to the University of Missouri-Rolla. Some of the computations were performed on the NSF sponsored supercomputer center in Ithaca, NY.

#### References

- Batra, R. C., and Jayachandran, R., 1992, "Effect of Constitutive Models on Steady State Axisymmetric Deformations of Thermoelastic-Viscoplastic Targets," *Int. J. Impact Engr.*, Vol. 12, pp. 209-226.
- Batra, R. C., and Liu, D. S., 1989, "Adiabatic Shear Banding in Plane Strain Problems," *ASME Journal of Applied Mechanics*, Vol. 56, pp. 527-534.
- Bodner, S. R., and Partom, Y., 1975, "Constitutive Equations for Elastic-Viscoplastic Strain-Hardening Materials," *ASME Journal of Applied Mechanics*, Vol. 42, pp. 385-389.
- Brown, S. B., Kim, K. H., and Anand, L., 1989, "An Internal Variable Constitutive Model for Hot Working of Metals," *Int. J. Plasticity*, Vol. 5, pp. 95-130.
- Budiansky, B., 1970, "Thermal and Thermoelastic Properties of Isotropic Composites," *J. Comp. Mat.*, Vol. 4, pp. 286-295.
- Gear, C. W., 1971, *Numerical Initial Value Problems in Ordinary Differential Equations*, Prentice-Hall, Englewood Cliffs, NJ.
- Giovanola, J. H., 1988, "Adiabatic Shear Banding Under Pure Shear Loading," *Mech. Materials*, Vol. 7, pp. 59-87.
- Hindmarsh, A. C., 1983, "ODEPACK, A Systematized Collection of ODE Solvers," *Scientific Computing*, R. S. Stepleman et al., eds., North-Holland, Amsterdam, pp. 55-64.

- Inoue, T., 1989, "Inelastic Constitutive Relationships and Applications to Some Thermomechanical Processes Involving Phase Transformations," *Thermal Stresses III*, R. B. Hetnarski, ed., North-Holland, Amsterdam, pp. 192-278.
- Lindholm, U. S., and Johnson, G. R., 1983, "Strain-Rate Effects in Metals at Large Strain Rates," *Material Behavior Under High Stresses and Ultrahigh Loading Rates*, J. Mescall and V. Weiss, eds., Plenum Press, NY, pp. 61-79.
- Massey, H. F., 1921, "The Flow of Metal During Forging," *Proc. Manchester Assoc. Engineers*, pp. 21-26.
- Reed-Hill, R. E., 1973, *Physical Metallurgy Principles*, Van Nostrand Co., New York.
- Roger, H. C., 1979, "Adiabatic Plastic Deformation," *Anin. Rev. Mat. Sci.*, Vol. 9, pp. 283-319.
- Tresca, H., 1878, "On Further Application of the Flow of Solids," *Proc. Inst. Mech. Engr.*, Vol. 30, pp. 301-345.
- Wingrove, A. L., 1971, "A Note on the Structure of Adiabatic Shear Bands in Steel," Tech. Memo 33, Australian Defence Scientific Service, Defence Standards Lab., Department of Supply, Maribyrnong, Victoria.
- Yu, H. J., Wolfstieg, U., and Macherauch, E., 1979, "Berechnung der Abschreckeigenspannungen in Stahlzylindern unter Berücksichtigung der Umwandlungsvorgänge," *Arch. Eisenhüttenwes.*, Vol. 50, pp. 81-84.
- Zener, C., and Hollomon, J. H., 1944, "Effect of Strain Rate Upon Plastic Flow of Steel," *J. Appl. Phys.*, Vol. 15, pp. 22-32.
- Zhu, Z. G., and Batra, R. C., 1990, "Dynamic Shear Band Development in Plane Strain Compression of a Viscoplastic Body Containing a Rigid Inclusion," *Acta Mechanica*, Vol. 84, pp. 89-107.